processes

MDPI

Article

Pressure-Dependent Pore-Scale Remobilization of Remaining Oil by CO_2 Flooding in Waterflooded Tight Sandstone

Huohai Yang [1], Lei Dai [1], Xiaohui Zhang [2], Yuchen Zhang [2], Ming Zhang [2], Bin Wang [2], Ming Gu [2], Juntao Cui [2] and Renze Li [1,*]

[1] Petroleum and Natural Gas Engineering College, Southwest Petroleum University, Chengdu 610050, China
[2] Research Institute of Exploration and Development, PetroChina Changqing Oilfield Company, Xi'an 710018, China
* Correspondence: lrzswpu@163.com

Abstract

Waterflooding in tight sandstone reservoirs preferentially mobilizes oil in large, well-connected pores, leaving substantial remaining oil in medium–small and poorly connected pore spaces. In this study, specific Chang 6 tight sandstone cores from the Ordos Basin were investigated using high-temperature and high-pressure online NMR displacement experiments, combined with CO_2–oil phase behavior tests and CO_2–brine–rock interaction experiments. The minimum miscibility pressure of the crude oil–CO_2 system was estimated to be 19.4 MPa based on the available slim-tube data. CO_2 dissolution enhanced oil mobility through swelling and viscosity reduction, while CO_2–brine–rock reactions increased core permeability by 18.24–25.55%. Compared with waterflooding, CO_2 flooding increased average oil mobilization in large, medium, and small pores by 33.66%, 39.56%, and 22.20%, respectively. Medium pores contributed most to incremental recovery, whereas small-pore oil was activated mainly under higher pressure. These results indicate that CO_2 flooding can enhance recovery in the tested waterflooded Chang 6 tight sandstone cores by improving crude-oil mobility, modifying pore-throat connectivity, and expanding displacement from large pores to medium–small pores.

Keywords: tight sandstone reservoir; CO_2 flooding; waterflooding; remaining oil; oil mobilization; pore-scale mobilization; online NMR

1. Introduction

Tight sandstone reservoirs have become important targets for unconventional petroleum development because of their large resource potential and wide distribution. However, their low porosity, low permeability, fine pore throats, strong heterogeneity, and poor fluid mobility seriously restrict effective displacement and pressure maintenance during production [1,2]. The Chang 6 reservoir of the Yanchang Formation in the Ordos Basin is a typical tight sandstone reservoir in China, characterized by complex pore-throat structures, strong microscopic heterogeneity, and limited fluid flow capacity [3–5]. Although waterflooding is widely applied in the development of low-permeability and tight sandstone reservoirs, injected water commonly advances preferentially through large pores, microfractures, and well-connected flow channels, resulting in limited sweep efficiency and substantial remaining-oil retention in medium–small pores, dead-end pores, and poorly connected pore systems [6,7]. Previous NMR-based displacement and imbibition studies have shown that pore structure, injection pressure, wettability, and pore-throat connectivity

Check for updates

Academic Editor: Qingbang Meng

Received: 18 May 2026
Revised: 17 June 2026
Accepted: 17 June 2026
Published: 23 June 2026

Copyright: © 2026 by the authors. Licensee MDPI, Basel, Switzerland. This article is an open access article distributed under the terms and conditions of the Creative Commons Attribution (CC BY) license.

jointly control waterflooding efficiency and remaining-oil distribution in tight sandstone cores [8–13]. In addition, SEM, MICP, X-ray micro-CT, digital rock, and pore-scale visualization studies have demonstrated that remaining oil in tight reservoirs is highly dispersed and strongly affected by pore-throat geometry, connectivity, and two-phase flow behavior [14–18]. Recent work on droplet falling-film evaporation over micro–nano-structured horizontal tubes has shown that transient film thickness is strongly governed by droplet topological evolution and pulsation effects, indicating that interfacial dynamics should be considered when analyzing local liquid-film distribution and heat-transfer enhancement [19]. Such oil-film formation can reduce oil-phase connectivity and increase the difficulty of mobilizing remaining oil in confined pore spaces. Moreover, wettability heterogeneity and water invasion may further reduce oil-phase conductivity and aggravate water-blocking damage, making remaining oil trapped in restricted pore spaces difficult to produce by continued water injection [20,21]. Therefore, for waterflooded Chang 6 tight sandstone reservoirs, the key challenge lies not only in the inherently poor flow capacity of tight pore systems, but also in the pore-scale retention and limited remobilization of remaining oil, which creates a strong demand for effective follow-up enhanced oil recovery methods after waterflooding.

CO_2 injection has been widely considered an effective follow-up method for improving oil recovery in tight reservoirs. Compared with water, CO_2 can dissolve into crude oil, induce oil swelling, reduce oil viscosity, lower interfacial resistance, and improve oil mobility. When the injection pressure approaches or exceeds the minimum miscibility pressure, CO_2–oil mass transfer is strengthened, and the displacement process may gradually shift from immiscible to near-miscible or miscible conditions, thereby improving displacement efficiency [22]. In addition, CO_2 dissolved in formation water can react with reactive minerals, causing local mineral dissolution, pore-throat modification, and permeability variation, which may improve the accessibility of previously unswept pore spaces [23,24]. Previous studies on CO_2 flooding, CO_2-WAG, and miscible or near-miscible CO_2 displacement have confirmed the potential of CO_2-EOR in tight and low-permeability reservoirs, but they also show that the recovery response is strongly controlled by reservoir quality, pressure condition, injection mode, and pore-scale heterogeneity [25–30]. Recent NMR-based and high-temperature/high-pressure visualization studies further indicate that CO_2 injection can enhance pore-scale oil mobilization in tight reservoirs, and that miscibility condition, injection pressure, and pore-throat structure jointly determine the mobilization efficiency of micro- and nano-scale pore oil [31,32].

Although the enhanced recovery potential of CO_2 has been widely recognized, several key issues remain insufficiently understood for waterflooded tight sandstone reservoirs. First, many previous studies have focused on bulk recovery improvement, whereas quantitative pore-scale comparisons of oil mobilization after waterflooding are still limited. Second, the contribution of different pore systems, especially large, medium, and small pores, to incremental recovery during CO_2 flooding has not been clearly distinguished. Third, the pressure-dependent transition from immiscible to near-miscible or miscible CO_2 flooding and its influence on pore-scale remaining-oil remobilization require further clarification under unified experimental conditions. Therefore, it is necessary to establish a direct link between waterflooding-induced remaining-oil occurrence and CO_2-induced pore-scale remobilization.

To address these issues, this study takes the Chang 6 tight sandstone reservoir in the Ordos Basin as the research object and establishes an integrated experimental framework combining waterflooding limitation evaluation, CO_2–oil phase-behavior experiments, CO_2–brine–rock reaction experiments, and high-temperature high-pressure online NMR displacement tests. The objectives of this study are to: (1) clarify the mechanism by which

waterflooding fails to effectively mobilize remaining oil in medium–small pores; (2) quantify the pore-scale mobilization characteristics of remaining oil during CO_2 flooding after waterflooding; and (3) reveal the effects of reservoir quality and injection pressure on CO_2 flooding performance. The results provide a pore-scale experimental basis for optimizing CO_2-EOR injection pressure and development strategies in waterflooded tight sandstone reservoirs.

2. Materials and Methods

2.1. Geological Background and Core Samples

Tight sandstone core samples were collected from the Chang 6 reservoir of the Yanchang Formation in the Ordos Basin, China. The target reservoir is an important tight-oil interval in the basin and is dominated by fine-grained lithic feldspathic sandstone, with locally developed very fine-grained lithic feldspathic sandstone, siltstone, and minor calcareous-cemented sandstone. It is characterized by low porosity, low permeability, fine pore throats, strong heterogeneity, and poor fluid mobility, making it suitable for investigating the remobilization of remaining oil after waterflooding (see Table 1).

Table 1. Basic properties and displacement scheme of representative cores used in online NMR flooding experiments.

Core No.	Reservoir Class	Permeability (mD)	Porosity (%)	CO_2 Flooding Pressure (MPa)	Displacement Scheme
S1	Class I	0.1742	12.83	10, 15, 20	Waterflooding followed by CO_2 flooding
S2	Class II	0.1179	9.42	10, 15, 20	Waterflooding followed by CO_2 flooding
S3	Class III	0.0811	6.58	10, 15, 20	Waterflooding followed by CO_2 flooding

All experimental cores were taken from physical core samples of the Chang 6 reservoir, with burial depths ranging from approximately 1872.72 to 2682.40 m. To evaluate the influence of reservoir quality on waterflooding and subsequent CO_2 flooding, representative cores were classified into Class I, Class II, and Class III reservoirs. The classification was based on petrological characteristics, pore-throat structure, oil-bearing properties, and crude-oil occurrence state, including grain size and sorting, detrital composition, interstitial material content, residual primary intergranular pores, secondary dissolution pores, microfractures, pore connectivity, fluorescent area, bitumen content, and dominant oil-bearing pore spaces.

As shown in Figure 1, Class I cores represent relatively high-quality reservoirs with better pore connectivity and more developed dissolution pores or microfractures. Class II cores represent intermediate-quality reservoirs with moderate storage and flow capacity. Class III cores represent relatively poor-quality reservoirs with finer pore throats, weaker connectivity, and stronger flow resistance.

2.2. Experimental Program

The experimental program was designed to clarify the limitations of waterflooding, the interaction mechanisms between CO_2 and reservoir fluids/rocks, and the pore-scale remobilization characteristics of remaining oil during CO_2 flooding after waterflooding. The experiments were divided into three modules: waterflooding limitation evaluation, CO_2–oil/rock interaction experiments, and high-temperature and high-pressure online NMR displacement experiments (see Table 2).

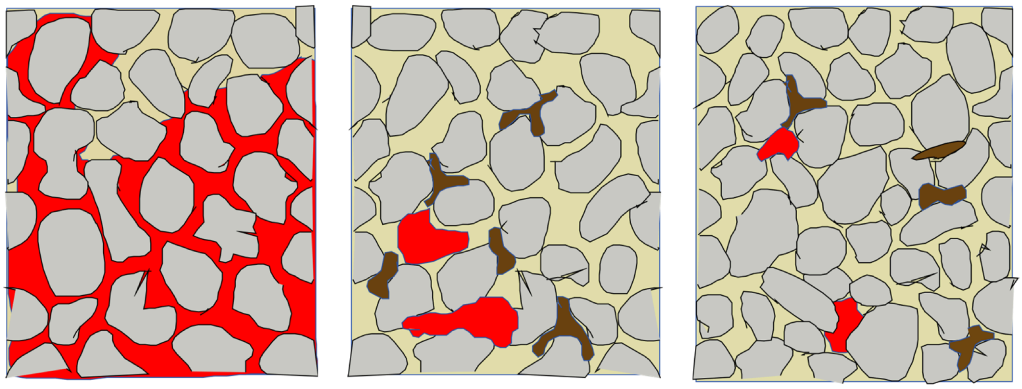

(**a**) Type I reservoir (**b**) Type II reservoir (**c**) Type III reservoir

Figure 1. Schematic diagram illustrating the mechanism of reservoir classification.

Table 2. Experimental program and analytical purpose.

Experimental Module	Methods	Number of Samples
Waterflooding limitation evaluation	Spontaneous imbibition wettability test	10 tests
	Water-locking evaluation experiment	10 tests
	Oil–water relative permeability test	9 tests
CO_2 interaction experiments	CO_2–brine–rock reaction experiment	2 tests
	CO_2–oil swelling experiment	1 test
	Slim-tube test	1 test
Pore-scale displacement experiment	High-temperature and high-pressure online NMR displacement experiment	9 tests

The waterflooding limitation evaluation included spontaneous imbibition wettability tests, water-locking evaluation experiments, and oil–water relative permeability tests. These experiments were used to identify the main factors restricting oil production during waterflooding, including wettability heterogeneity, water-blocking damage, and the reduction in oil-phase flow capacity after water invasion.

The CO_2 interaction experiments included slim-tube tests, CO_2–oil swelling and viscosity-reduction experiments, and CO_2–brine–rock reaction experiments. These experiments were used to evaluate the minimum miscibility pressure, the improvement in crude-oil mobility caused by CO_2 dissolution, and the influence of CO_2–brine–rock reactions on pore-throat connectivity and permeability.

The high-temperature and high-pressure online NMR displacement experiments were the core experimental method in this study. They were conducted to dynamically monitor the redistribution and production of crude oil during waterflooding and subsequent CO_2 flooding, and to quantify the degree of oil mobilization in different pore-size ranges.

2.3. High-Temperature and High-Pressure Online NMR Displacement Procedure

High-temperature and high-pressure online NMR displacement experiments were conducted to monitor the dynamic redistribution and production of crude oil during waterflooding and subsequent CO_2 flooding under simulated reservoir conditions. The experiments were designed to quantify the recovery response and pore-scale oil mobilization characteristics of tight sandstone cores after different displacement stages.

Before displacement, the core samples were cleaned to remove remaining oil, dried to a constant weight, and then vacuumed. Deuterium oxide-based simulated formation water was used as the aqueous phase during core saturation and waterflooding to suppress the NMR response of the water phase. Because D_2O has a negligible proton signal in low-field

proton NMR measurements, the measured T_2 spectra mainly reflected the distribution and variation of crude oil in the pore system. After vacuuming, the cores were saturated with D_2O and then displaced or saturated with crude oil to establish the initial oil-bearing state. The initial NMR T_2 spectrum was acquired after oil saturation and used as the reference state for subsequent recovery and pore-scale mobilization calculations.

Waterflooding was first performed to simulate the primary displacement process and to establish the remaining-oil distribution after water injection. The waterflooding experiment was conducted at a temperature of 89.35 °C, a confining pressure of 5 MPa, and an injection rate of 0.01 mL/min. D_2O was injected as the water phase until no further oil production occurred. After waterflooding, the NMR T_2 spectrum was measured again to determine the remaining-oil distribution in different pore-size ranges.

After the waterflooding stage, CO_2 flooding was conducted to further mobilize the remaining oil. The CO_2 injection pressures were set at 10, 15, and 20 MPa to evaluate the pressure-dependent remobilization behavior of remaining oil. These pressure levels were selected to represent different displacement conditions relative to the measured minimum miscibility pressure of the crude oil–CO_2 system. CO_2 was injected at 0.1 mL/min until there was no further oil production. After CO_2 flooding, the final NMR T_2 spectrum was recorded to quantify the additional oil mobilized from different pore-size classes.

For each core-flooding test, NMR T_2 spectra were acquired at three key states: after oil saturation, after waterflooding, and after CO_2 flooding. The reduction in the integrated T_2 spectral area between different displacement stages was used to calculate the recovery factor, while the variation in T_2 spectral area within different relaxation-time intervals was used to evaluate the mobilization degree of oil in small, medium, and large pores. This procedure allowed the displacement efficiency of waterflooding and CO_2 flooding to be compared at both the whole-core scale and the pore-size scale.

2.4. NMR Data Processing and Evaluation Indicators

High-temperature and high-pressure online NMR displacement experiments were conducted to monitor the dynamic redistribution and production of crude oil during waterflooding and subsequent CO_2 flooding. Before displacement, the core samples were cleaned, dried, vacuumed, saturated with simulated formation water, and then saturated with crude oil to establish the initial oil-bearing state. NMR T_2 spectra were acquired after oil saturation, after waterflooding, and after CO_2 flooding. The displacement temperature, confining pressure, injection pressure, injection rate, and injected pore volume were set according to the simulated reservoir conditions.

Under the same lithology and surface relaxivity conditions, the NMR T_2 relaxation time is positively correlated with pore radius. Therefore, fluids in small pores generally correspond to short T_2 components, whereas fluids in large and well-connected pores correspond to long T_2 components. Based on the calibration between NMR T_2 spectra and pore-throat characterization results, the pores were divided into three classes: small pores with $T_2 \leq 1$ ms, medium pores with 1 ms < $T_2 \leq 100$ ms, and large pores with $T_2 > 100$ ms. The same classification criterion was applied to all cores and displacement stages to ensure comparability.

The recovery factor was calculated from the reduction in the integrated T_2 spectral area. The waterflooding recovery factor, incremental recovery factor during CO_2 flooding, and total recovery factor were calculated as follows:

$$E_w = \frac{A_0 - A_w}{A_0} \times 100\%$$
$$\Delta E_{CO_2} = \frac{A_w - A_c}{A_0} \times 100\%$$
$$E_t = \frac{A_0 - A_c}{A_0} \times 100\%$$

where A_0, A_w, A_c are the integrated T_2 spectral areas after oil saturation, after waterflooding, and after CO_2 flooding, respectively. E_w is the waterflooding recovery factor, ΔE_{CO_2} is the incremental recovery factor during CO_2 flooding, and E_t is the total recovery factor.

To quantify oil mobilization in different pore-size ranges, the mobilization degree of each pore class was calculated using the T_2 spectral area within the corresponding interval:

$$\eta_{i,t} = \frac{A_{i,0} - A_{i,t}}{A_{i,0}} \times 100\%$$

where i represents small, medium, or large pores; $A_{i,0}$ is the initial T_2 spectral area of pore Class I after oil saturation; and $A_{i,t}$ is the T_2 spectral area of the same pore class after a given displacement stage.

3. Results

3.1. Waterflooding Performance and Remaining-Oil Distribution

As shown in Figure 2, waterflooding experiments showed clear differences in oil recovery among the three reservoir types. The waterflooding recovery factors of Class I, Class II, and Class III cores were 38.57%, 22.68%, and 17.56%, respectively. The recovery factor decreased with deteriorating reservoir quality, indicating that pore-throat structure and connectivity strongly controlled the primary waterflooding efficiency.

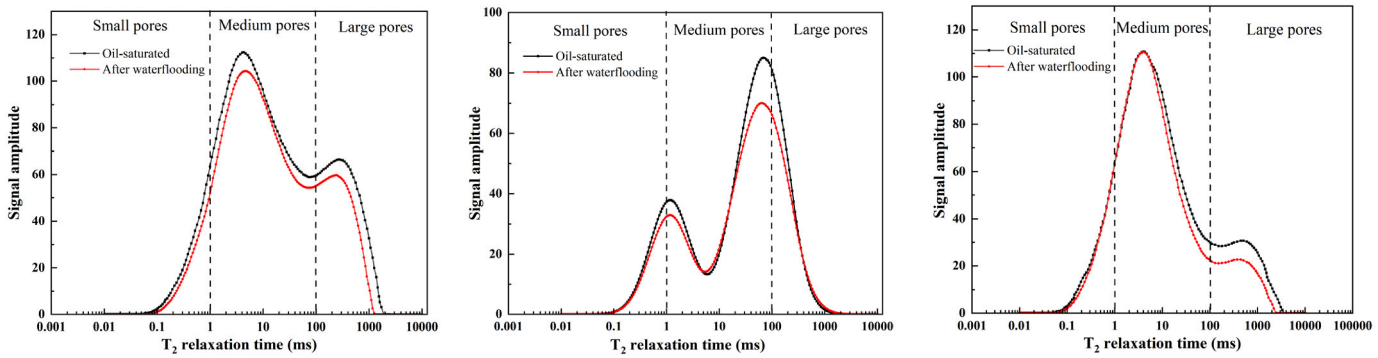

Figure 2. NMR T_2 curves of different reservoir-class cores after waterflooding: (**a**) Class I core; (**b**) Class II core; (**c**) Class III core.

The NMR results further revealed that waterflooding mobilized oil selectively in different pore-size ranges. For the Class I core, the degree of oil mobilizations in small, medium, and large pores were 6.29%, 14.77%, and 42.53%, respectively. For the Class II core, the corresponding values were 12.11%, 23.05%, and 18.21%, respectively. For the Class III core, the values were 8.34%, 13.21%, and 22.04%, respectively. Overall, waterflooding mainly mobilized oil in relatively large pores and well-connected flow channels, whereas oil in medium–small pores remained less effectively displaced (see Table 3).

Table 3. Waterflooding recovery factors of the three types of cores.

Core No.	Displacement Pressure Difference (MPa)	Mobilization Degree of Small Pores (%)	Mobilization Degree of Medium Pores (%)	Mobilization Degree of Large Pores (%)	Recovery Factor (%)
S1	5	6.29	14.77	42.53	38.57
S2	5	12.11	23.05	18.21	22.68
S3	5	8.34	13.21	22.04	17.56

The oil–water relative permeability curves further confirmed the flow limitation during waterflooding. As shown in Figure 3, oil-phase relative permeability decreased rapidly with increasing water saturation, indicating that the effective oil-flow capacity was strongly weakened after water entered the pore network. This reduction in oil-phase conductivity limited the continuous displacement of oil, especially in tight pore-throat systems with poor connectivity.

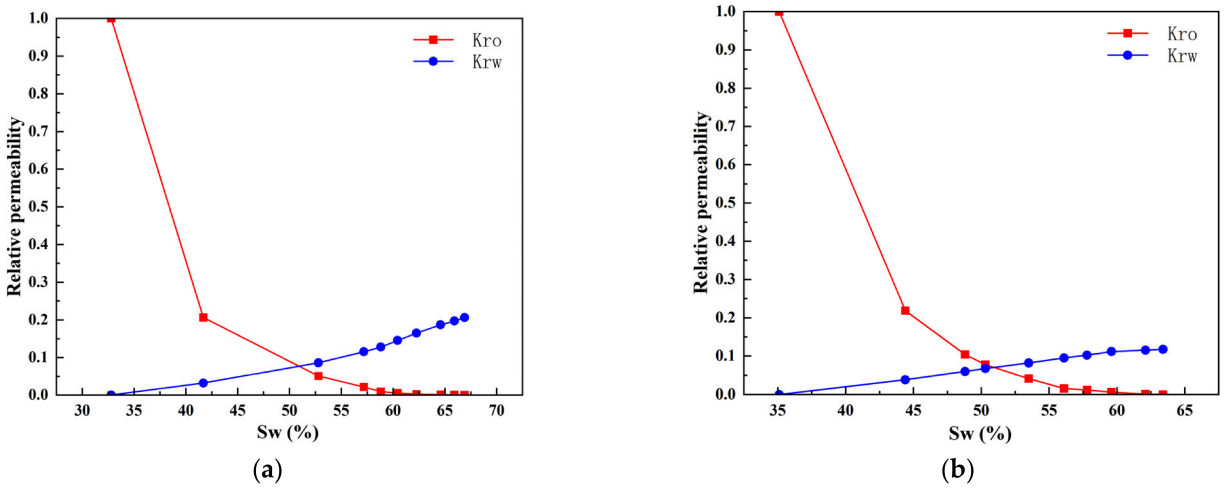

Figure 3. Oil–water relative permeability curves of tight sandstone cores. (**a**) Sample 1; (**b**) Sample 2.

The spontaneous imbibition tests showed that the tight sandstone samples were generally weakly water-wet, with local wettability heterogeneity. Such wettability conditions favored non-uniform water invasion and the formation of preferential flow paths during waterflooding. Meanwhile, the water-locking evaluation indicated that water invasion caused significant permeability damage in tight cores. Typical water-locking samples showed an average permeability damage degree of 82.69%, while transition-type samples generally showed damage degrees of 65–80%. These results indicate that waterflooding not only had limited sweep efficiency but also further restricted oil mobility by reducing oil-phase connectivity and increasing flow resistance in narrow pore throats.

These results demonstrate that waterflooding mainly establishes dominant flow channels in large pores, while substantial remaining oil is remaining in medium–small pores, poorly connected pore spaces, and restricted pore-throat systems.

3.2. CO_2–Oil and CO_2–Rock Interaction Characteristics

The slim-tube test showed that the minimum miscibility pressure of the crude oil–CO_2 system was 19.4 MPa at 89.35 °C. The current formation pressure of the target reservoir is approximately 17.456 MPa, which is close to the near-miscible pressure range. This result indicates that the reservoir has the pressure basis for developing near-miscible or miscible CO_2 flooding when the injection pressure is increased (see Figure 4).

The CO_2–oil swelling experiment showed that CO_2 dissolution significantly changed crude-oil properties. With increasing CO_2 mole fraction, the saturation pressure of the crude oil increased from 8.21 MPa to 30.25 MPa, while the oil volume factor increased from 1.21 to 1.79. At 40 MPa, the crude-oil viscosity decreased from 1.66 mPa·s to 0.24 mPa·s, corresponding to a maximum viscosity reduction of 80.89%. These results demonstrate that CO_2 can improve crude-oil mobility through oil swelling and viscosity reduction (see Figure 5).

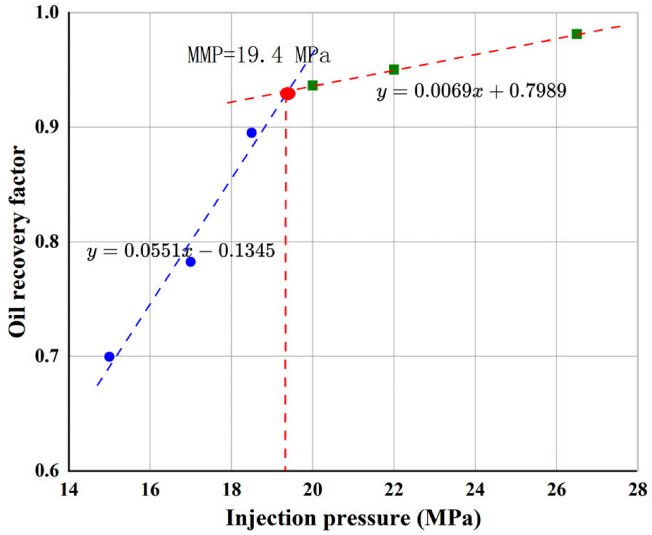

Figure 4. Determination of the minimum miscibility pressure (MMP) from the relationship between oil recovery factor and CO_2 injection pressure.

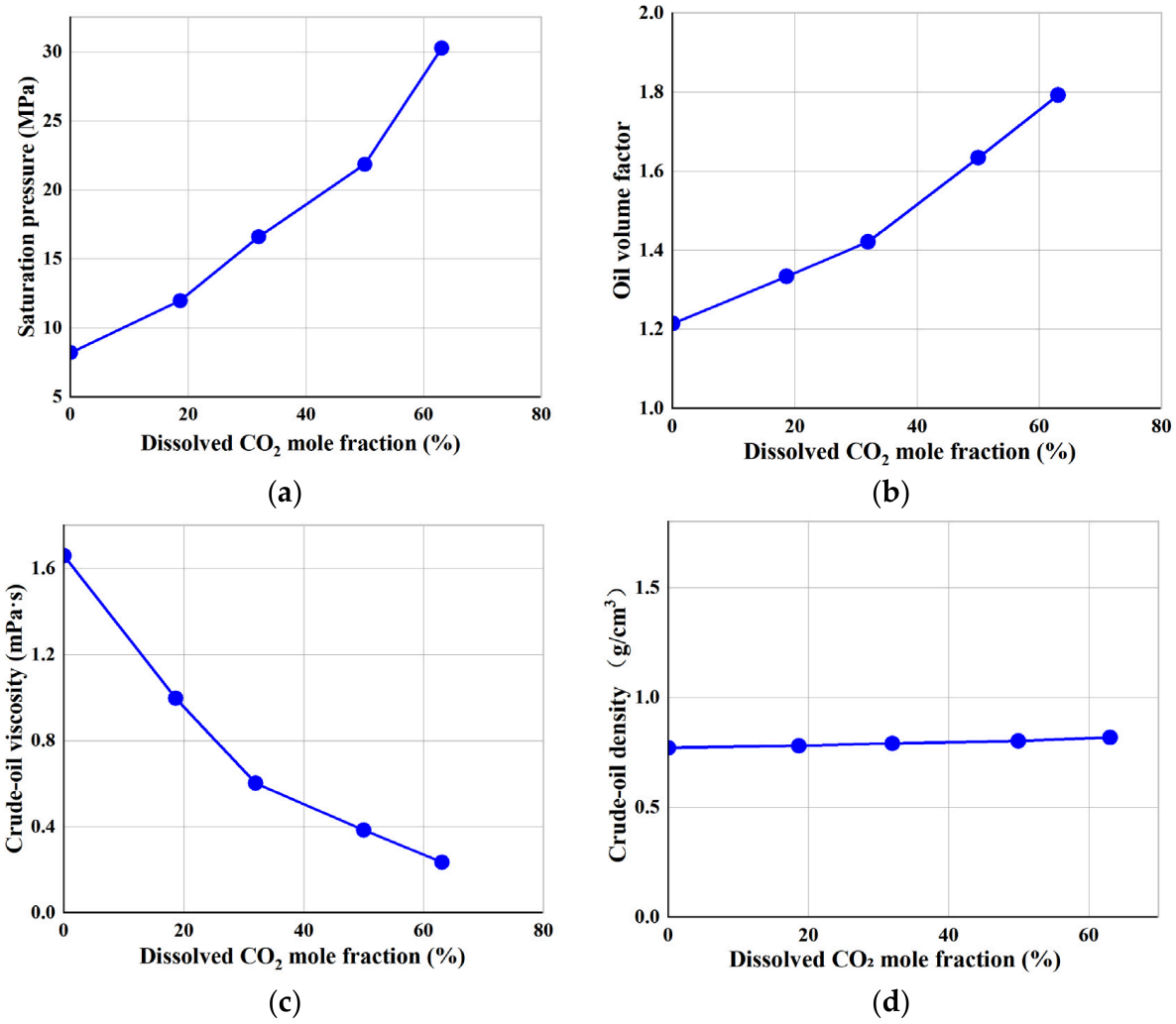

Figure 5. Effects of CO_2 dissolution on crude-oil physical properties. (**a**) Saturation pressure; (**b**) oil volume factor; (**c**) crude-oil viscosity; (**d**) crude-oil density.

The CO_2–brine–rock reaction experiments showed that CO_2 also affected the pore-throat system. After reaction, the absolute permeability of two representative cores increased from 0.09367 mD to 0.1176 mD and from 0.2357 mD to 0.2787 mD, respectively. The corresponding permeability increments were 25.55% and 18.24%. Microscopic observations showed that feldspar and some carbonate minerals were dissolved after CO_2–brine–rock interaction, forming local dissolution pores, microfractures, and improved pore connectivity (see Figure 6).

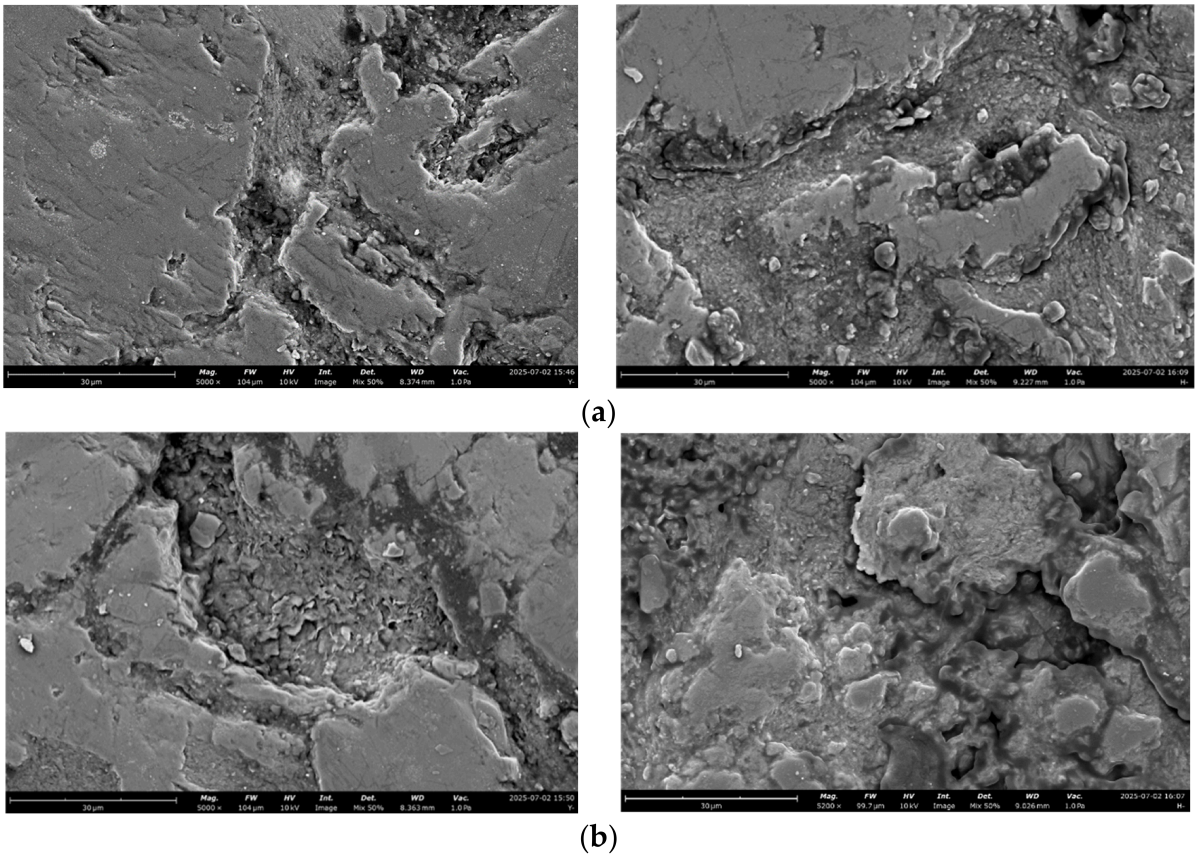

Figure 6. SEM images of pore-throat structures before and after CO_2–water–rock interaction. (**a**) Before interaction; (**b**) after interaction.

These results indicate that CO_2 can influence both the fluid phase and the rock pore system. The oil swelling, viscosity reduction, near-miscible pressure condition, and local permeability improvement together provide the physical basis for further mobilizing remaining oil after waterflooding.

3.3. Pressure-Dependent Recovery During CO_2 Flooding After Waterflooding

After waterflooding, subsequent CO_2 flooding improved the recovery factors of all three reservoir types. However, the magnitude of recovery improvement varied with reservoir quality and injection pressure.

At 10 MPa, the final recovery factors of Class I, Class II, and Class III cores were 43.56%, 36.84%, and 28.97%, respectively. Compared with the waterflooding stage, the corresponding incremental recovery factors were 4.99, 14.16, and 11.41%. This indicates that even under relatively low-pressure conditions, CO_2 flooding could further mobilize part of the remaining oil after waterflooding.

When the injection pressure increased to 15 MPa, the final recovery factors of Class I, Class II, and Class III cores increased to 65.91%, 62.99%, and 52.41%, respectively. The

corresponding increments, relative to waterflooding, were 27.34, 40.31, and 34.85%. The recovery improvement was much greater than that at 10 MPa, indicating a stronger pressure-dependent response of CO_2 flooding.

At 20 MPa, the final recovery factors further increased to 78.45%, 73.25%, and 69.14% for Class I, Class II, and Class III cores, respectively. Compared with waterflooding, the recovery factors increased by 39.88, 50.57, and 51.58%, respectively. Among the three reservoir types, Class I cores maintained the highest final recovery factor under all pressure conditions, whereas Class II and Class III cores showed larger incremental recovery at higher pressure.

Overall, the recovery response showed a positive correlation with injection pressure. The pressure interval from 15 MPa to 20 MPa was particularly important for recovery enhancement. Although high-quality reservoirs had higher final recovery factors, medium- and low-quality reservoirs exhibited greater incremental recovery potential after pressure elevation (see Figure 7).

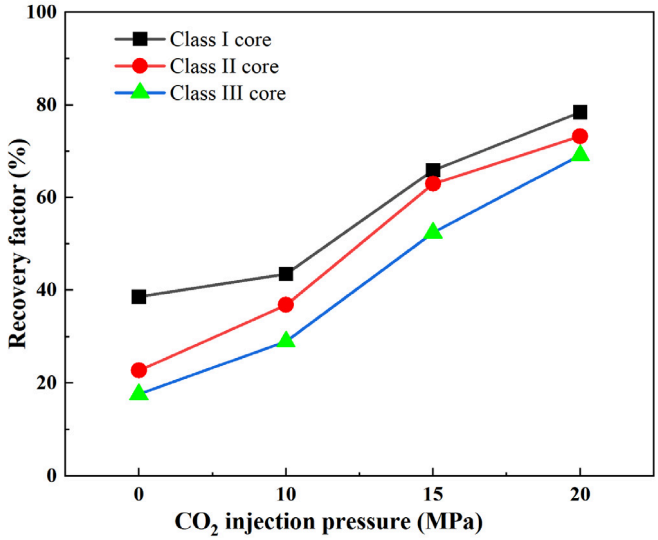

Figure 7. Recovery factors after waterflooding and subsequent CO_2 flooding at different injection pressures for different core classes.

3.4. Pore-Scale Mobilization of Remaining Oil by CO_2 Flooding

The online NMR displacement experiments further quantified the contribution of different pore-size classes to oil mobilization during waterflooding and subsequent CO_2 flooding. The results showed that CO_2 flooding enhanced oil mobilization in large, medium, and small pores, but the degree of improvement varied significantly among pore classes and injection pressures.

For the Class I core, the degree of oil mobilizations in small, medium, and large pores increased from 6.29%, 14.77%, and 42.53% after waterflooding, to 14.50%, 22.10%, and 55.86% at 10 MPa CO_2 flooding, respectively. When the pressure increased to 15 MPa, the mobilization degrees further increased to 25.94%, 70.27%, and 75.12%. At 20 MPa, they reached 41.18%, 84.47%, and 84.06%, respectively. These results indicate that CO_2 flooding first improved oil mobilization in large pores and then substantially enhanced mobilization in medium pores as pressure increased (see Figure 8).

For the Class II core, the degree of oil mobilizations in small, medium, and large pores were 12.11%, 23.05%, and 18.21% after waterflooding. After CO_2 flooding at 10 MPa, they increased to 25.13%, 38.50%, and 34.89%, respectively. At 15 MPa, the values increased to 53.36%, 76.21%, and 59.21%. At 20 MPa, they further increased to 69.03%, 83.50%, and

71.85%. The Class II core showed a strong response in both medium and small pores, especially under medium- and high-pressure conditions (see Figure 9).

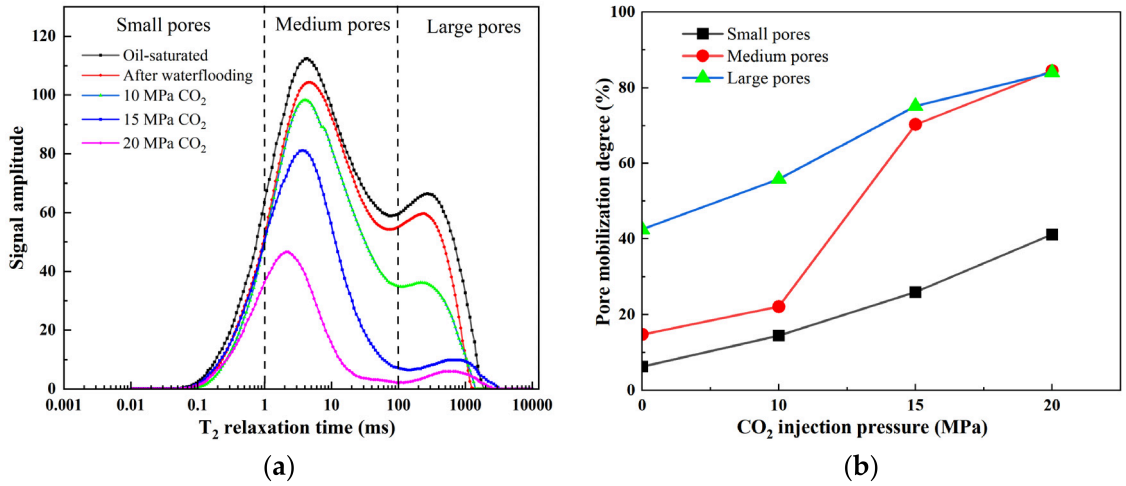

(**a**) (**b**)

Figure 8. Pore mobilization characteristics of Class I cores during CO_2 flooding. (**a**) NMR T_2 spectra under different displacement stages; (**b**) mobilization degree of different pore-size classes at different CO_2 injection pressures.

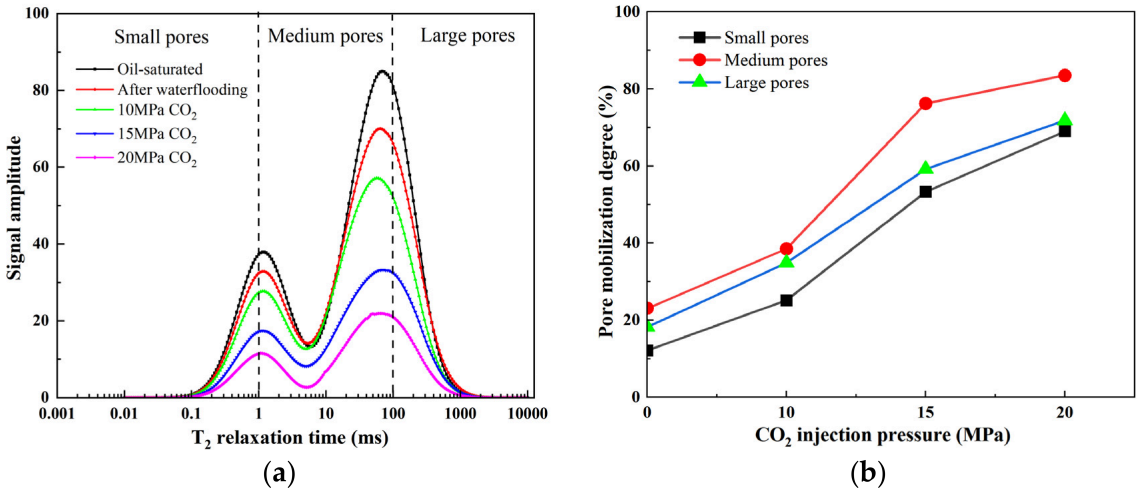

(**a**) (**b**)

Figure 9. Pore mobilization characteristics of Class II cores during CO_2 flooding. (**a**) NMR T_2 spectra under different displacement stages; (**b**) mobilization degree of different pore-size classes at different CO_2 injection pressures.

For the Class III core, the degree of oil mobilizations in small, medium, and large pores were 8.34%, 13.21%, and 22.04% after waterflooding. At 10 MPa CO_2 flooding, the values increased slightly to 9.36%, 19.07%, and 32.45%, respectively. At 15 MPa, they increased to 12.01%, 47.86%, and 60.04%. At 20 MPa, the mobilization degrees reached 29.52%, 67.16%, and 77.84%, respectively. These results show that pressure increase was especially important for improving oil mobilization in the poorer-quality reservoir (see Figure 10).

Compared with waterflooding, CO_2 flooding increased the average degree of oil mobilization in large, medium, and small pores by 33.66%, 39.56%, and 22.20%, respectively. Among the three pore-size classes, medium pores showed the largest average improvement, indicating that they were the main contributor to incremental recovery during CO_2 flooding after waterflooding. Large pores were further swept by CO_2 along existing flow paths, whereas small pores were significantly mobilized only under higher-pressure conditions.

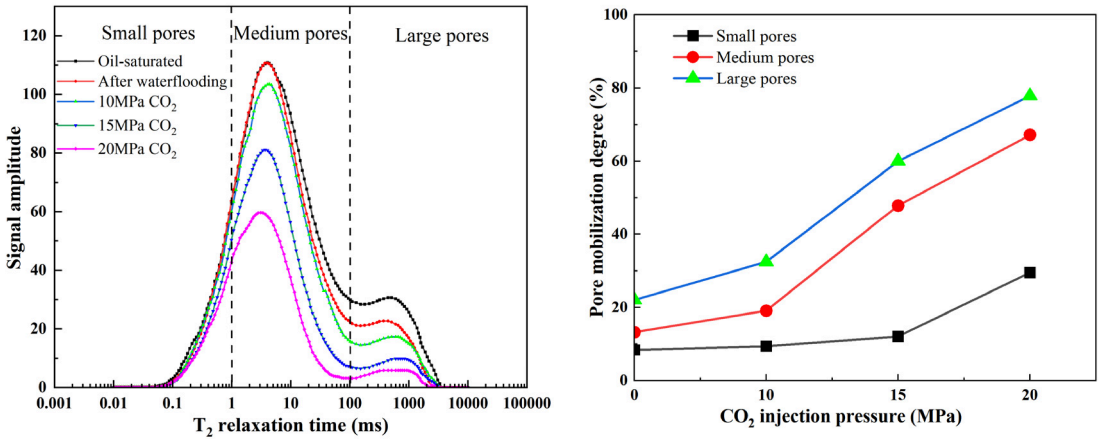

Figure 10. Pore mobilization characteristics of Class III cores during CO_2 flooding. (**a**) NMR T_2 spectra under different displacement stages; (**b**) mobilization degree of different pore-size classes at different CO_2 injection pressures.

In summary, the NMR results demonstrate that waterflooding mainly mobilized oil in large and relatively well-connected pores, while CO_2 flooding expanded the effective displacement range toward medium and small pores. The pore-scale mobilization process evolved from supplementary displacement in large pores at low pressure to dominant mobilization in medium pores at intermediate pressure and further activation of small pores at high pressure.

4. Discussion

4.1. Mechanism of Waterflooding-Induced Remaining-Oil Enrichment

Waterflooding-induced remaining-oil enrichment in tight sandstone reservoirs is mainly governed by preferential flow, reduced oil-phase conductivity, capillary trapping, and water-locking damage. Due to small pore throats, poor connectivity, and strong heterogeneity, injected water preferentially flows through large pores and well-connected seepage channels rather than forming a uniform displacement front. Consequently, oil in large pores is more readily displaced, whereas oil in medium–small pores, narrow throats, and dead-end spaces remain insufficiently contacted.

Relative permeability, water-locking, and imbibition results jointly support this mechanism. The rapid decline in oil-phase relative permeability indicates that continuous oil-flow pathways are easily disrupted after water invasion. Meanwhile, water remaining in narrow throats increases the threshold pressure for oil remobilization and further weakens oil-phase connectivity. Weak water-wetness with local wettability heterogeneity also promotes uneven water invasion and non-uniform sweep.

Therefore, remaining oil after waterflooding is not merely bypassed oil, but the result of preferential water invasion, oil-flow pathway disconnection, capillary retention, and water-blocking damage. Large pores and dominant channels become the main water-flow pathways, while medium–small and poorly connected pores become the primary regions of remaining-oil enrichment (see Figure 11).

4.2. Mechanism of CO_2-Induced Remobilization of Remaining Oil

CO_2 flooding can effectively remobilize remaining oil after waterflooding because it acts not only as a displacement fluid but also as an active medium that alters crude-oil properties, phase behavior, and local pore-throat conditions. After dissolving into crude oil,

CO_2 causes oil swelling and viscosity reduction, which improves oil mobility, lowers flow resistance, and facilitates the reconnection of trapped oil.

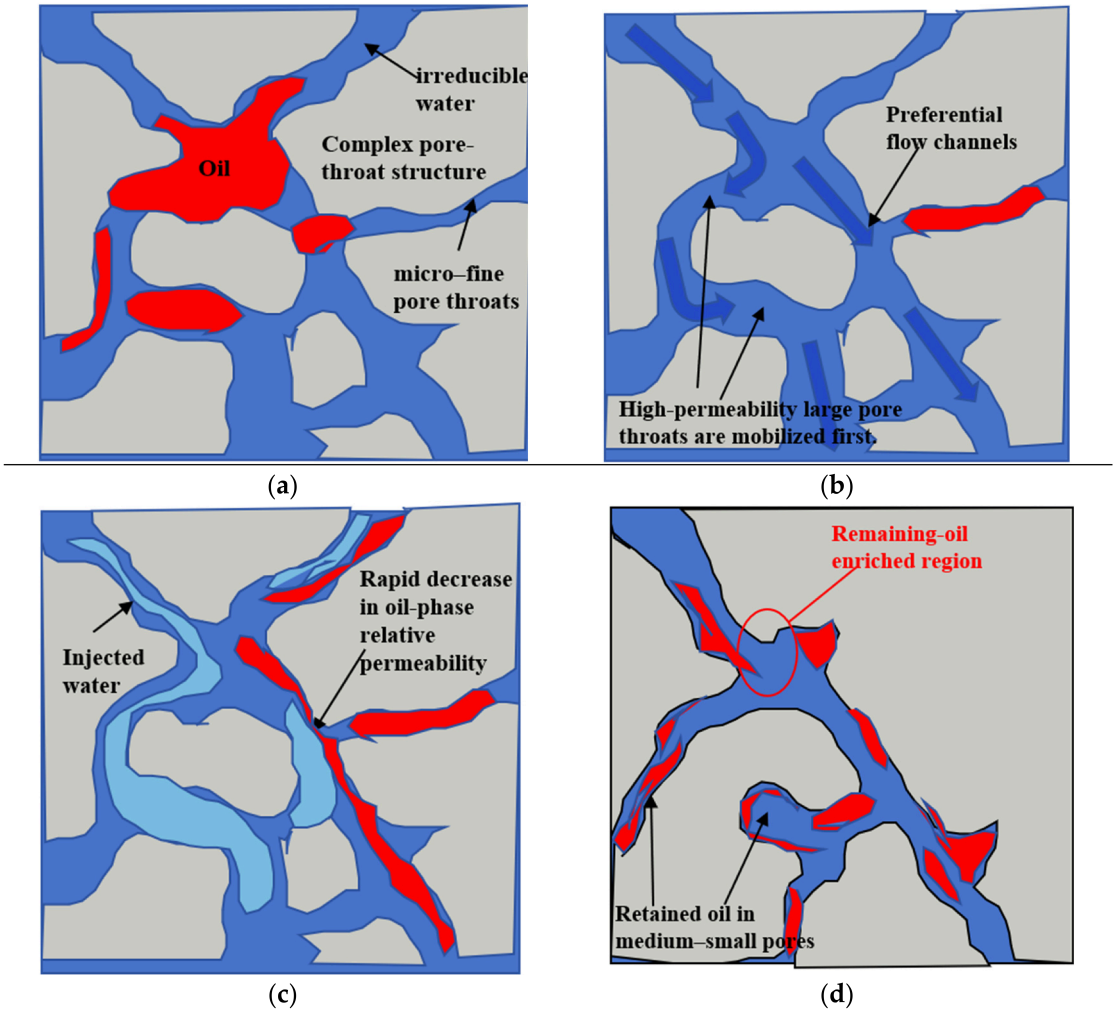

Figure 11. Schematic illustration of waterflooding-induced remaining-oil enrichment in tight sandstone pore-throat networks. (**a**) Initial oil distribution; (**b**) formation of preferential flow channels; (**c**) waterflooding-induced flow restriction; (**d**) remaining-oil enrichment.

The measured minimum miscibility pressure of the crude oil–CO_2 system was 19.4 MPa. As injection pressure approaches or exceeds this value, CO_2–oil mass transfer is strengthened, interfacial resistance decreases, and displacement gradually shifts from immiscible toward near-miscible or miscible conditions. This weakens capillary trapping and enhances the mobilization of oil remaining in restricted pore spaces.

In addition, CO_2–brine–rock reactions may locally improve pore-throat connectivity through mineral dissolution, providing additional pathways for CO_2 migration. NMR results further indicate that CO_2 first supplements displacement in large pores and connected channels, then increasingly mobilizes medium-pore oil as pressure rises, and finally activates part of the small-pore oil under higher-pressure conditions.

Thus, CO_2 flooding enhances recovery by expanding the effective displacement range from large pores to medium and small pores through the coupled effects of oil-property improvement, phase-behavior regulation, pore-throat modification, and multi-scale oil remobilization.

4.3. Implications for Injection-Pressure Optimization

Injection pressure strongly controls the recovery response and pore-scale oil mobilization of CO_2 flooding after waterflooding. Because the minimum miscibility pressure was 19.4 MPa, the tested pressures represent different displacement states.

At 10 MPa, CO_2 flooding is mainly immiscible. Oil recovery increment is limited, and mobilization occurs primarily in large pores and connected flow channels. At 15 MPa, enhanced CO_2 dissolution and mass transfer improve the displacement efficiency, especially for medium-pore remaining oil. At 20 MPa, the pressure exceeds the minimum miscibility pressure, allowing near-miscible or miscible displacement to dominate. Under this condition, interfacial resistance is further reduced, medium-pore mobilization remains high, and part of the small-pore oil is also activated (see Figure 12).

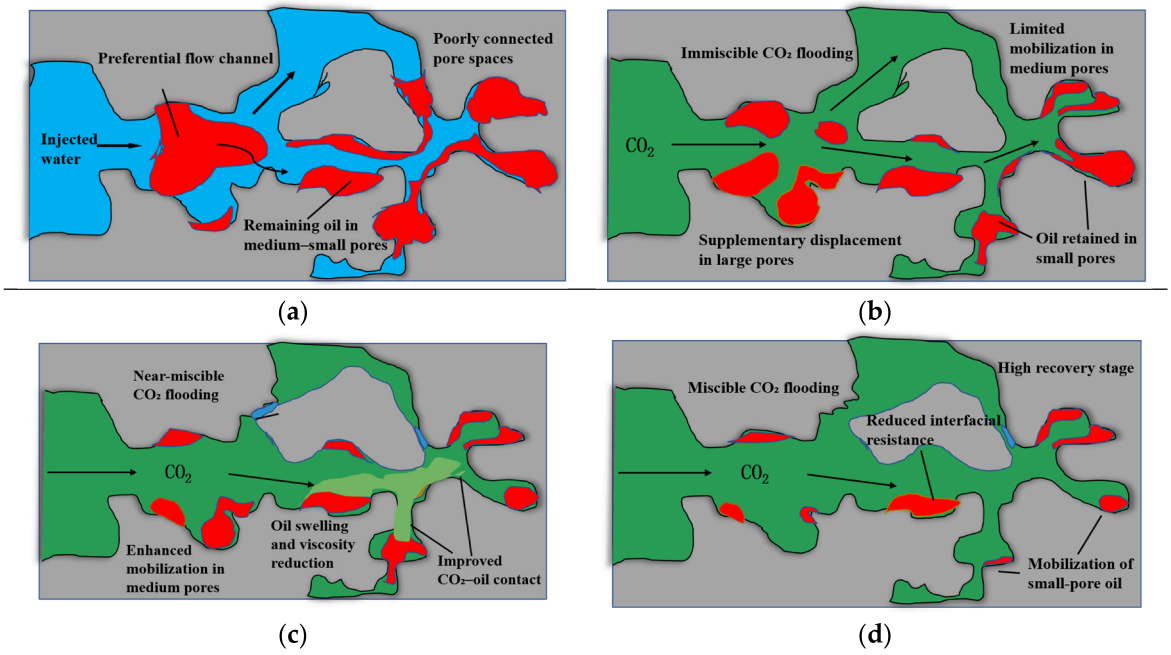

Figure 12. Schematic illustration of pore-scale oil mobilization mechanisms during CO_2 flooding after waterflooding. (**a**) Waterflooding stage; (**b**) immiscible CO_2 flooding; (**c**) near-miscible CO_2 flooding; (**d**) miscible CO_2 flooding.

Reservoir quality also affects the pressure response. Class I cores show higher final recovery because of better connectivity, whereas Class II and Class III cores exhibit larger incremental recovery at elevated pressure, suggesting greater pressure-sensitive remaining-oil potential in poorer-quality reservoirs.

Overall, low-pressure CO_2 flooding mainly supplements displacement in large pores, intermediate pressure effectively mobilizes medium-pore remaining oil, and near-miscible or miscible flooding further activates small-pore oil. Therefore, maintaining injection pressure close to or slightly above the minimum miscibility pressure is favorable for maximizing remaining-oil remobilization and improving CO_2-EOR performance in waterflooded tight sandstone reservoirs.

5. Conclusions

This study investigated the pressure-dependent pore-scale remobilization of remaining oil during CO_2 flooding after waterflooding in tight sandstone reservoirs. By integrating waterflooding limitation evaluation, CO_2–oil phase-behavior experiments, CO_2–brine–rock interaction tests, and high-temperature and high-pressure online NMR displacement ex-

periments, the effects of reservoir quality, injection pressure, and pore-size distribution on remaining-oil mobilization were systematically analyzed. The results clarify how waterflooding-induced preferential flow controls the distribution of remaining oil and how subsequent CO_2 flooding improves oil recovery by enhancing crude-oil mobility, modifying pore-throat connectivity, and expanding displacement from large pores to medium–small pores. The main conclusions are as follows:

(1) Waterflooding mainly mobilized oil in large pores and well-connected dominant flow channels, whereas a considerable amount of remaining oil remained in medium–small pores and poorly connected pore spaces. This indicates that conventional waterflooding has limited effectiveness in improving the microscopic sweep efficiency of tight sandstone reservoirs after the formation of preferential flow paths.

(2) The minimum miscibility pressure of the crude oil–CO_2 system was determined to be 19.4 MPa, indicating that CO_2 flooding under near-miscible conditions can effectively improve oil displacement efficiency. CO_2 enhanced crude-oil mobility through oil swelling, viscosity reduction, and mass transfer between CO_2 and crude oil, thereby promoting the remobilization of remaining oil after waterflooding.

(3) CO_2–water–rock interactions improved the pore-throat seepage capacity of tight sandstone cores through mineral dissolution and pore-structure modification. After CO_2 treatment, the core permeability increased by 18.24–25.55%, demonstrating that CO_2 flooding can not only displace remaining oil but also improve local flow conductivity in tight reservoirs.

(4) Compared with waterflooding, CO_2 flooding significantly enhanced the degree of oil mobilization in pores of different scales. The average degree of oil mobilization in large, medium, and small pores increased by 33.66%, 39.56%, and 22.20%, respectively, among which medium pores made the greatest contribution to incremental oil recovery.

(5) Miscible CO_2 flooding further improved oil recovery after waterflooding, with an incremental recovery of 47.34%. These results confirm that CO_2 flooding is an effective enhanced oil recovery method for waterflooded Chang 6 tight sandstone reservoirs, and that optimizing injection pressure is essential for improving the mobilization of remaining oil, especially in medium–small pores.

Author Contributions: Conceptualization, H.Y. and Y.Z.; Methodology, H.Y., X.Z. and Y.Z.; Investigation, H.Y., X.Z., B.W. and R.L.; Data curation, L.D. and R.L.; Formal analysis, L.D. and J.C.; Validation, L.D., X.Z., B.W. and R.L.; Software, J.C.; Visualization, J.C.; Resources, M.Z., B.W. and M.G.; Supervision, Y.Z., M.Z. and M.G.; Project administration, M.Z. and M.G.; Writing—original draft, H.Y.; Writing—review and editing, L.D., X.Z., Y.Z., M.Z., B.W., M.G., J.C. and R.L. All authors have read and agreed to the published version of the manuscript.

Funding: This research received no external funding.

Data Availability Statement: The original contributions presented in this study are included in the article. Further inquiries can be directed to the corresponding author.

Conflicts of Interest: Authors Xiaohui Zhang, Yuchen Zhang, Ming Zhang, Bin Wang, Ming Gu and Juntao Cui were employed by Research Institute of Exploration and Development, PetroChina Changqing Oilfield Company, Xi'an, China. The remaining authors declare that the research was conducted in the absence of any commercial or financial relationships that could be construed as a potential conflict of interest.

References

1. Jia, C.Z.; Jiang, L.; Zhao, W. Tight oil and gas in total petroleum system: Accumulation mechanism, enrichment laws and resource prospects. *Acta Pet. Sin.* **2025**, *46*, 1–16, 47. [CrossRef]

2. Zhu, R.K.; Li, G.X.; Cui, J.W.; Huang, F.; Lu, X.; Guo, Z.; Cao, Z. Geological conditions and exploration prospects of tight oil and gas in China. *Acta Pet. Sin.* **2025**, *46*, 17–32. [CrossRef]
3. Chen, Y.; Feng, C.; Wei, D.; Wang, C.; He, Y.; Ge, Y.; Li, X.; Hao, S.; Fan, X.; Wei, W. Formation, distribution and exploration strategies of tight oil in the Chang 6 Member of the Triassic Yanchang Formation in southeastern Ordos Basin. *Acta Pet. Sin.* **2025**, *46*, 335–354. [CrossRef]
4. Liu, H.L.; Yang, Y.Y.; Wang, F.Q.; Deng, X.; Liu, Y.; Nan, J.; Wang, J.; Zhang, H. Micro pore and throat characteristics and origin of tight sandstone reservoirs: A case study of the Triassic Chang 6 and Chang 8 members in Longdong area, Ordos Basin, NW China. *Pet. Explor. Dev.* **2018**, *45*, 223–234. [CrossRef]
5. Li, P.; Ou, Y.; Chen, H.; Li, Q.; Zhao, L.; Yan, J. Pore throat distributions and movable fluid occurrences in different diagenetic facies of tight sandstone reservoirs in the Triassic Chang 6 reservoirs, Wuqi Area, Ordos Basin, China. *J. Pet. Explor. Prod. Technol.* **2024**, *14*, 1783–1797. [CrossRef]
6. Wang, X.Z.; Dang, H.L.; Gao, T. Method of moderate water injection and its application in ultra-low permeability oil reservoirs of Yanchang Oilfield, NW China. *Pet. Explor. Dev.* **2018**, *45*, 1094–1102. [CrossRef]
7. Li, J.J.; Liu, Y.; Gao, Y.J.; Cheng, B.; Meng, F.; Xu, F. Effects of microscopic pore structure heterogeneity on the distribution and morphology of remaining oil. *Pet. Explor. Dev.* **2018**, *45*, 1112–1122. [CrossRef]
8. Yang, Y.; Xiao, W.; Bernabe, Y.; Xie, Q.; Wang, J.; He, Y.; Li, M.; Chen, M.; Ren, J.; Zhao, J.; et al. Effect of pore structure and injection pressure on waterflooding in tight oil sandstone cores using NMR technique and pore network simulation. *J. Pet. Sci. Eng.* **2022**, *217*, 110886. [CrossRef]
9. Jiang, Z.; Liu, Z.; Zhao, P.; Chen, Z.; Mao, Z. Evaluation of tight waterflooding reservoirs with complex wettability by NMR data: A case study from Chang 6 and 8 members, Ordos Basin, NW China. *J. Pet. Sci. Eng.* **2022**, *213*, 110436. [CrossRef]
10. Jiang, Z.; Li, G.; Zhao, P.; Zhou, Y.; Mao, Z.; Liu, Z. Study on spontaneous imbibition and displacement characteristics of mixed-wet tight sandstone reservoir based on high-precision balance and NMR method. *Fuel* **2023**, *345*, 128247. [CrossRef]
11. Wang, Y.; Ge, L.Z.; Lu, Y.; Zhang, Y. Fluid mobility and remaining oil occurrence characteristics in low-permeability sandstone based on NMR displacement experiments. *Pet. Geol. Recovery Effic.* **2023**, *30*, 22–31. [CrossRef]
12. Fu, L. Online NMR experiments on dynamic imbibition, drainage and displacement in tight sandstone: A case study of the Fuyu oil layer in northern Songliao Basin. *Daqing Pet. Geol. Dev.* **2023**, *42*, 66–74. [CrossRef]
13. Yu, Y.; Sun, Y.D.; Gao, R.; Da, L.; Hou, J.; Yang, M. Determination of surface relaxivity of tight cores based on T2 cutoff value. *Pet. Geol. Exp.* **2022**, *44*, 342–349. [CrossRef]
14. Su, Y.; Zha, M.; Jiang, L.; Ding, X.; Qu, J.; Jin, J.; Iglauer, S. Pore structure and fluid distribution of tight sandstone by the combined use of SEM, MICP and X-ray micro-CT. *J. Pet. Sci. Eng.* **2022**, *208*, 109241. [CrossRef]
15. Wang, R.; Zhang, Y.; Sun, C.; Li, J.; Meng, X.; Yang, C.; Chen, Z. A study on the remaining oil distribution in tight reservoirs based on a 3D pore structure model. *Processes* **2025**, *13*, 203. [CrossRef]
16. Liu, C.; Yin, Y.; Bai, R.; Liu, D. Pore-scale imaging of oil-brine movement during waterflooding with wettability alteration from tight sandstone. *Improv. Oil Gas Recovery* **2023**, *7*, 1–10. [CrossRef]
17. Yi, X.; Zhang, M.; Mu, G. Microscopic distribution and development strategy of remaining oil in tight sandstone. *Processes* **2023**, *11*, 1907. [CrossRef]
18. Fan, W.; Yu, H.; He, S.; Shi, J.; Wang, J.; Arif, M.; Wang, C.; Ding, S.; Zhang, Y. Micro-scale two-phase flow experiments and remaining oil distribution in tight sandstone. *Nat. Resour. Res.* **2025**, *34*, 3179–3192. [CrossRef]
19. Jia, B.; Zhao, Z.; Wang, X.; Chen, C.; Ma, X.; Wu, J.; Yang, L.; Politaeva, N. Local film thickness in relation to the droplet topological structure of droplet falling film on micro-nano structured horizontal tubes. *Case Stud. Therm. Eng.* **2026**, *83*, 108125. [CrossRef]
20. Liu, G.; Wang, H.; Tang, J.; Liu, Z.; Yang, D. Effect of wettability on oil and water distribution and production performance in a tight sandstone reservoir. *Fuel* **2023**, *341*, 127680. [CrossRef]
21. Fan, P.; Liu, Y.; He, Y.; Hu, Y.; Chao, L.; Wang, Y.; Liu, L.; Li, J. Experimental study on the mechanism and law of low-salinity water flooding for enhanced oil recovery in tight sandstone reservoirs. *ACS Omega* **2024**, *9*, 12665–12675. [CrossRef] [PubMed]
22. Zhu, W.Y.; Yue, M.; Liu, Y.F.; Liu, K.; Song, Z. Research progress in development theory of tight oil reservoirs in China. *Chin. J. Eng.* **2019**, *41*, 1103–1114. [CrossRef]
23. Lin, R.; Yu, Z.; Zhao, J.; Dai, C.; Sun, Y.; Ren, L.; Xie, M. Experimental evaluation of tight sandstones reservoir flow characteristics under CO_2-brine-rock multiphase interactions: A case study in the Chang 6 layer, Ordos Basin, China. *Fuel* **2022**, *309*, 122167. [CrossRef]
24. Lyu, L.G.; Zhang, T.; Li, J.; Sun, J.; Zheng, H.; Wang, G. Effects of reservoir mineral types on CO_2 displacement performance in tight oil reservoirs. *Daqing Pet. Geol. Dev.* **2023**, *42*, 159–168.
25. Huang, X.; Ni, J.; Li, X.; Xue, J.; Bai, M.; Zhou, T. CO_2 flooding mobilization characteristics and influencing factors of reservoirs with different microscopic pore structures in tight oil reservoirs. *Acta Pet. Sin.* **2020**, *41*, 853–864. [CrossRef]
26. Li, J.; Duan, J.J.; Yao, Z.J.; Li, N.; Chen, F.; Zhao, Y.; Zhao, Y. Analysis on Influence Factors of Enhanced Oil Recovery in CO_2 Flooding After Water Flooding in Low Permeability Reservoir. *Unconv. Oil Gas* **2017**, *4*, 45–52. [CrossRef]

27. Lei, X.H.; Zheng, Z.G.; Yu, G.M.; Zhang, K. Response characteristics of CO_2 water-alternating-gas flooding after waterflooding in ultra-low permeability reservoirs. *Spec. Oil Gas Reserv.* **2020**, *27*, 113–117.
28. Wang, Y.-F.; Li, Z.-Y.; Zhang, S.-M.; Liu, D.-X.; Ding, M.-C. Remaining oil distribution in models with different heterogeneities after CO_2 WAG injection: Visual research by nuclear magnetic resonance technique. *J. Cent. S. Univ.* **2021**, *28*, 1412–1421. [CrossRef]
29. Song, H.Z.; Yang, E.L.; Li, T.L.; Lin, T.; Sun, Y.; Zhang, X. Laboratory experiments and numerical simulation of water-alternating-gas flooding after waterflooding in offshore oilfields. *Contemp. Chem. Ind.* **2021**, *50*, 1171–1175. [CrossRef]
30. Yang, S.; Xu, Y.; Huang, Z.; Zhang, Q.; Liu, T.; Li, X. Application of CO_2 miscible flooding in ultra-low permeability beach-bar sand reservoir. *Front. Earth Sci.* **2022**, *10*, 970719. [CrossRef]
31. Zhang, Z.; Sun, J.; Niu, Z.; Tuo, Z.; Zhong, X.; Zheng, X.; Zhang, R. Experimental study on the influencing factors and pore production law of CO_2 huff-and-puff in tight sandstone reservoirs. *Sci. Rep.* **2025**, *15*, 3492. [CrossRef] [PubMed]
32. Wang, D.; Zhan, E.; Liu, L.; Pi, Y.; Li, Z. Study on CO_2 flooding crude oil production characteristics and factors affecting oil flooding efficiency in tight reservoirs. *ACS Omega* **2025**, *10*, 41076–41088. [CrossRef] [PubMed]

Disclaimer/Publisher's Note: The statements, opinions and data contained in all publications are solely those of the individual author(s) and contributor(s) and not of MDPI and/or the editor(s). MDPI and/or the editor(s) disclaim responsibility for any injury to people or property resulting from any ideas, methods, instructions or products referred to in the content.